IEEE Access
Multidisciplinary ⋮ Rapid Review ⋮ Open Access Journal

Received 13 October 2023, accepted 15 November 2023, date of publication 27 November 2023,
date of current version 5 December 2023.

Digital Object Identifier 10.1109/ACCESS.2023.3336942

RESEARCH ARTICLE

Effective Electrical Model of a Beverage Can as a Foreign Object in EV Wireless Charging

ALICIA TRIVIÑO[1], ELISEO VILLAGRASA[1], FABIO CORTI[2], (Member, IEEE), GABRIELE MARIA LOZITO[2], (Member, IEEE), AND ALBERTO REATTI[2], (Member, IEEE)

[1]Escuela de Ingenierías Industriales, Universidad de Málaga, 29071 Málaga, Spain
[2]School of Engineering, University of Florence, 50121 Florence, Italy

Corresponding author: Alicia Triviño (atc@uma.es)

This work was supported by Spanish Ministerio de Ciencia e Innovacion (MICINN) Project through "Proyectos de I+D+i—RTI Tipo A" Programme under Grant PID2019-110531-RA-I00/AEI/10.13039/501100011033.

ABSTRACT Wireless chargers for electric vehicles are usually based on a magnetic field between two coils to transfer power without cables. Metallic objects in the volume comprised among these coils affect the magnetic field, reduce the power transferred to the load, and also result in hazards. Therefore, the implementation of techniques suitable to detect foreign objects is mandatory. The accurate modelling of the objects can help in the precision of the methods used for their detection. In this paper, we accurately identify the equivalent electrical model of a specific foreign object. The main advantage of using this model consists of the possibility of evaluating the performance of the whole charging system by performing time-domain simulations instead of complex finite element analysis. This is of interest for techniques using sensing coils and for self-sensing approaches. In particular, we have modelled a beverage can, which is an object expected in typical EV wireless chargers. The model is validated by comparing simulations based on this model and experimental results. From this analysis, some hot areas where the object causes a higher impact are identified. The procedure can be extended to other objects.

INDEX TERMS Wireless charging, electric vehicle, foreign object detection, metal object detection, beverage can, electrical model.

I. INTRODUCTION

Electric Vehicles (EVs) are a feasible and sustainable transport solution to cope with the greenhouse emissions generated by fuel-based vehicles. Although the acquisition of EVs is increasing, their selling rate is still low due mainly to the cost of the batteries and the unavailability of charging infrastructures. To overcome these disadvantages, Wireless Power Transfer (WPT) is a suitable technology to increase the scenarios in which the EV may be charged and to do it without the user intervention [1]. By now, inductive charging is the most mature technology for charging vehicles without cables. Inductive charging relies on a pair of air-coupled coils (one on the pavement and another in the chassis of the EV). The primary coil generates a magnetic field, which traverses the area of a secondary coil so that a voltage is induced across the load cabled to the secondary coil.

Due to the use of a magnetic field for power transfer, there is a concern about the safety of EMF exposure [2] and the alterations it can suffer due to foreign objects. Metal objects in the areas separating the coils or close to those elements can exhibit eddy currents due to the variable magnetic field traversing them. This will affect power transfer and may even cause some hazards (fire, damages to the system, etc.). Thus, Metal Object Detection (MOD) techniques constitute a complementary technology to guarantee the proper functioning of EV wireless chargers [3]. In fact, SAE J2954 requires sensors to protect against hazardous consequences from metal objects [4]. With the release of this standard, MOD techniques are receiving increasing attention.

MOD techniques can be generally classified into three main groups: sensor-based solutions, self-sensing and

The associate editor coordinating the review of this manuscript and approving it for publication was Diego Masotti.

methods with additional sensing coils [5]. First, sensor-based solutions rely on auxiliary equipment to monitor the physical properties in the area between the two coils. Radar and infrared sensors or image processors belong to this category. Their performance is independent of WPT power level but it may be susceptible to environmental conditions and their cost is high. Second, self-sensing approaches analyse electrical measurements such as currents and voltages on the transmitter and receiver coils. As these measurements may be used to detect potential problems in a conventional power transfer without object, the cost and complexity of this type of method are low. Finally, the third type of MOD technique is based on the use of additional coils to measure the variations of their induced voltage or equivalent inductance. In these methods, there are two sets of coils: the power coils and the sensing coils. The placement of the sensing coils must be carefully considered as their number and position affect the precision of the method for detecting the metal object [6]. The combination of several techniques has also been addressed [7].

In any of these techniques, there must be a design process to determine the configuration to follow. The configuration mainly entails the definition of the position and types of the sensors for the sensor-based solutions, the electrical measurements to consider for the self-sensing approaches and the number, geometries and ubication of the sensing coils for the techniques based on sensing coils. The identification of the appropriate configuration is supported by the theoretical analysis of the system performance with objects. Thus, a precise model of the objects is essential to determine the optimised configuration. The incorporation of the object in the design of these MOD techniques is usually performed with two main approaches. The first one consists in modelling the object in a Finite Element Analysis (FEA) tool and then time-consuming simulations must be accomplished, as can be seen in [8], [9], [10], and [11]. In the second one, the authors consider an equivalent electrical model of the object as it is shown in [12], [13], and [14]. This last method is preferred due to the fastness it can provide. Table 1 summarizes the main features of MOD based on sensor coils that were evaluated with objects. Table 2 those based on self-sensing. References [15], [16], and [17] only rely on a FEM analysis to test their techniques, which are time-consuming.

As shown in [7], [18], and [19], these authors use models based only on physical shapes. These models do not include the electrical and magnetic characteristics of the objects, which could lead to a significant deviation between simulations and experimental results. Regarding those techniques evaluated with experimental tests, there are some authors who support their work using FEM, as stated in [5], [10], [20], [21], [22], [23], [24], [25], [26], [27], [28], [29], [30], [31], [32], [33], and [34]. However, the use of FEM is only focused on the validation of the developed FOD techniques rather than checking whether the implemented models can accurately characterize the object. In [25] and [35], the authors propose electrical models for the objects. These models are derived from FEM models, but their accuracy is not validated with experimental results.

As for the tested objects, most authors focused on detecting coins, metal sheets, metal bars, etc. A beverage can is also analysed in some works. This object is particularly significant because of its extensive use in urban areas and thus, the probability of interfering with a WPT is high.

When designing MOD algorithms, it is important to have precise physical models of the metal objects so that the effects on the sensing coils or on the system parameters can be estimated accurately. This work focuses on developing and evaluating an electrical model of a beverage can (one of the six generic items considered as potential metal objects in SAE J2954, such as a steel bar). Specifically, the contributions of this work are threefold:

- Providing an effective electrical model for a can-shaped object to be used for the design or testing of MOD techniques. The model is generated from the physical characterization of the object in a FEM tool. From this tool, an electrical model is derived. Then, the validity of the equivalent circuit for the object is verified by contrasting experimental and simulation results in terms of changes in the electrical parameters (current and voltage on the primary and secondary sides), which is one of the MOD techniques. In contrast to [38] and [39], this work has focused on a real object. The determination of an equivalent electrical model of the object is useful for the test of future MOD techniques (with sensing coils or self-sensing) in simulation tools.
- Validation of the proposed electrical model as a computationally efficient solution based to simulate the foreign object presence in the WPT system in the time-domain. This has been accomplished for a wide range of scenarios with the can in different positions, resulting in shorter computational times when compared to FEM.
- Analysis of the impact of this object on the power transfer and identification of the areas that are most affected by it. The study has been done in a representative configuration of a Series-Series wireless charger. With this analysis, the effectiveness of the self-sensing approach is evaluated. Currents and voltages are measured and derived in the simulation tool, as these parameters are commonly used in self-sensing approaches as shown in Table 2.

Although this paper focuses on a can-shaped object, the procedure described (physical characterization and derivation of the electrical model) can be applied to other objects.

The remainder of the paper is structured as follows. Section II describes the equivalent circuit of the charger with a metal object. Section III develops the electrical model of the beverage can. Section IV describes the EV wireless charger where the model of the can is validated. The results of the experimental validation of the model proposed are

TABLE 1. Comparative of main features of MOD techniques based on sensor coils.

Ref.	Electrical model	Objects included in FEM	Objects tested experimentally	Validation of the electrical model	Power coil geometry	Compensation	Sensing coil geometry
[13]	×	×	A coin	×	Squared	N.S.	Squared array sensor
[15]	×	Aluminum cylinder, similar to a **beverage can**	×	×	Circular	S-S	Squared array sensor
[17]	×	A metal bar	×	×	Rectangular	LCC-LCC	Symmetrical rectangular array sensor
[18]	×	×	A coin and a paper clip	×	Circular	N.S.	Squared array sensor
[6]	×	A 5 cent coin, two different size **aluminum rods**, and an aluminum sheet	A **beverage can**, a 5 cent coin and an aluminum sheet	×	Circular	P-P	Two circular coils
[20]	×	A coin, a steel bar and a cuboid shape	A coin, a steel bar and a cuboid shaped	×	Circular	S-S	Circular array sensor
[21]	×	A coin and a set of coins	A coin and a set of coins	×	Rectangular	LCC-S	Two mesh coils
[22]	×	**Aluminum cylinder** and iron cylinder	**Aluminum cylinder** and iron cylinder	×	Squared	LCC-LCC	Squared array sensor
[23]	×	A copper cylinder	A copper cylinder	×	Circular	S-S	Two mesh coils
[24]	×	Metal bar	Metal bar	×	Rectangular	N.S.	Symmetric squared array sensor
[29]	×	A metal bar	A steel pan	×	Circular	N.S.	Four rectangular coils
[30]	×	×	A metal sheet, a set of ferrites and a smartphone	×	N.S.	N.S.	Array of straight conductors
[31]	×	A metal bar	A coin, a key and a **beverage can**	×	N.S.	LCL-S	Squared array sensor
[32]	×	A coin	A coin	×	Squared	N.S.	Circular array sensor
[33]	×	Aluminum plate	Aluminum and copper plates	×	Rectangular	LCC-S	A continuous bipolar coil conforming a net
[5]	×	A coin	A coin	×	DD	S-S	Symmetrical rectangular array
[34]	×	A coin	A coin, A nail and a **beverage can**	×	DD	S-S	Rectangular array sensor
[35]	Conductivity derived from FEM model	×	A coin, a bolt, a **beverage can** and a gum wrapper	×	Rectangular	S-S	Symmetric rectangular array sensor
[36]	×	×	A round **aluminum bar**	×	N.S.	N.S.	Squared array sensor

*N.S.= Not Specified.

detailed in Section V. Finally, Section VI summarizes the main conclusions of this paper.

II. THEORETICAL ANALYSIS

The structure of the EV wireless charger utilized in the proposed analysis is shown in Fig. 1. The primary side is assumed to be on the pavement. It requires some power converters to adapt the frequency of the electrical signal to the one required by the EV wireless charger (typically 85 kHz [4]). The secondary side corresponds to the electronics on the EV. The core of this schematic is composed of two coupled coils (L_1 and L_2) and their parasitic resistances (R_1 and R_2). M_{12} corresponds to the mutual inductance between the transmitter and the receiver. As a representative structure, the matching networks are composed of capacitors C_1 and C_2 in series with the coils. The secondary side also has some power electronics to adjust the features of the current and voltage to the requirements of the battery. To guarantee adequate charging, the wireless charger is equipped with some controllers. The controller can either adjust the setting of the power converters or interrupt the power transfer when some dangerous events are detected (e.g. excessive voltage/current in one component, presence of a metal object). The controllers may be installed on the primary, secondary or both sides [40]. For an illustrative goal, in the present work the controller is installed on the primary side of the system but it may require measurements from the secondary side. We have added

TABLE 2. Comparative of main features of MOD techniques based on self-sensing.

Ref.	Electrical model	Objects included in FEM	Objects tested experimentally	Validation of the electrical model	Power coil geometry	Compensation	Parameter measurements considered
[7]	×	×	A coin, a **beer can**, two different coils and a ferrite cylinder	×	Circular	S-S	Sending a high frequency signal through the coils and sensing the variations of their impedance
[10]	×	**Aluminum disk**	**Aluminum disk**	×	Circular	N.S.	Measurement of variation of the self-impedance and transimpedance
[16]	×	A dielectric sphere	×	×	Helical	N.S.	Detection of variations of the transmitter's impedance based on variations of the electromagnetic field
[19]	×	×	A copper piece and a water bottle	×	Rectangular	N.S.	Power spectral density estimation based on measurements of the transmitter's current
[25]	Resistance and inductance derived from FEM model	A copper plate, a copper coin and an iron coin	A copper plate, a copper coin and an iron coin	×	Rectangular	S-S	Measurements of the impedances supported by a particle swarm optimization algorithm
[26]	×	**Aluminum bar** and iron bar	**Aluminum bar** and iron bar	×	Circular	S-S	Detection of resonance frequency deviation
[27]	×	Iron bar	**Beverage can**	×	Squared transmitter, circular receiver	LCC-S	Measurements of the transmitter's current assisted by machine learning tools
[28]	×	5 cents coin	5 cents coin	×	Circular	S-S	Detection of resonance frequency deviation
[37]	×	×	Steel sheet	×	Rectangular	S-S	Measurement of the transmitter's impedance deviation using transmission-side voltage pulses
Proposal	**Resistance and inductance derived from real measurements**	**Beverage can**	**Beverage can**	✓	**Rectangular**	**S-S**	**Voltage's and current's magnitude and phase deviation of the transmitter and receiver coils**

*N.S.= Not Specified.

a secondary controller to collect and transmit the data. Anyway, the proposed procedure is valid with other types of controllers.

The output of the primary converter (V_{inv}) is a sinusoidal wave of 85 kHz. However, due to the use of compensation systems, the first harmonic approximation is valid. Thus, the system is analysed with a sine-wave generator, referred to as the phasor $\vec{V}_{inv}$ in Fig. 2. The rms value of this phasor is $\vec{V}_{inv,rms} = \frac{4V_{inv}}{\sqrt{2}\pi}$. The impedance of the battery at the input of the secondary rectifier is modelled as the resistance R_L (referred to as the equivalent load resistance). The relationship between the internal resistance of the battery (R_{bat}) and R_L is $R_L = 8R_{bat}/\pi^2$. Assuming that there is no object, it is possible to derive the following equations with a mesh-based analysis:

$$\vec{V}_{inv} = \left(R_1 + j\omega L_1 + \frac{1}{j\omega C_1}\right)\vec{I}_1 - j\omega M_{12}\vec{I}_2 \tag{1}$$

$$\vec{V}_2 = \left[(R_2 + j\omega L_2)\,\vec{I}_2 - j\omega M_{12}\vec{I}_1\right] = \left(R_L + \frac{1}{j\omega C_2}\right)\vec{I}_2 \tag{2}$$

The previous model and the circuital equations change when there is a metal object between the two coils. The object is modelled with an additional mesh [3], as shown in Fig. 1. This new mesh is composed of an inductance coupled with the primary and secondary coils (L_{MO}) and a resistance (R_{MO}). The mutual inductances M_{1O} and M_{2O} depend on the position of the object in the area of the power transfer.

With simple circuital re-arrangement of the elements, it is possible to include the new mesh in the original two-coils configuration, deriving the circuit in Fig. 2, as used in [41]. The values of these components in the simplified model are:

$$Z'_{11} = Z_{11} + \frac{\omega^2 M_{1O}^2}{Z_{MO}} \tag{3}$$

$$Z'_{22} = Z_{22} + \frac{\omega^2 M_{2O}^2}{Z_{MO}} \tag{4}$$

$$M'_{12} = M_{12}\left(1 - \frac{K_{1O}K_{2O}}{K_{12}}\right) = M_{12} * \beta_M \tag{5}$$

where $Z_{MO} = j\omega L_{MO} + R_{MO}$, $Z_{11} = j\omega L_1 + 1/j\omega C_1 + R_1$, $Z_{22} = j\omega L_2 + 1/j\omega C_2 + R_2 + R_L$ and K_{12}, K_{1O} and K_{2O}

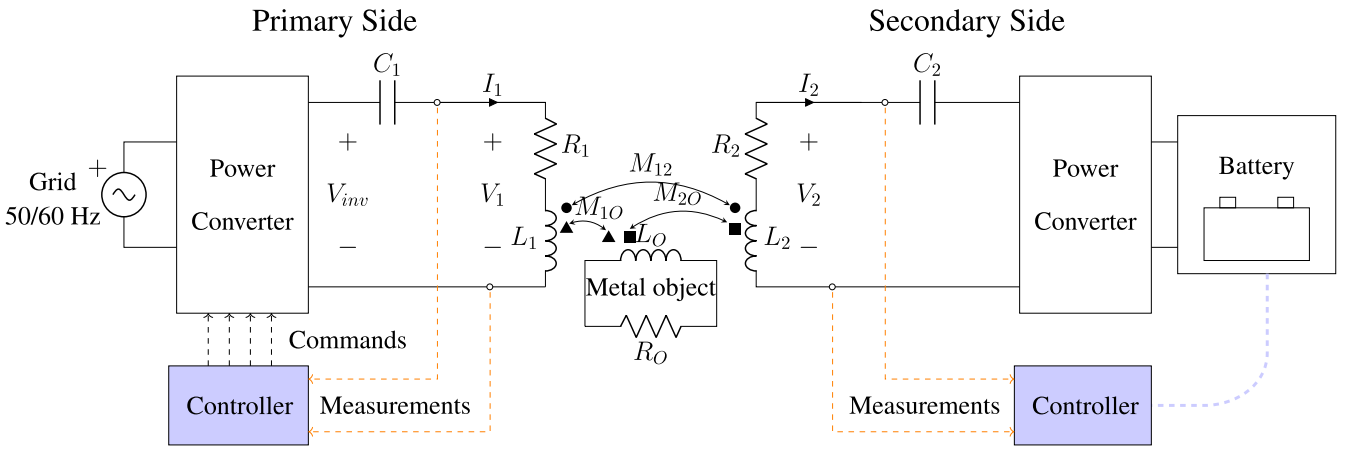

FIGURE 1. Generic diagram for an EV wireless charger with a metal object.

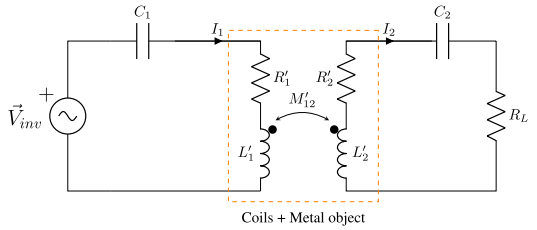

FIGURE 2. Simplified equivalent circuit of a coupler with a metal object.

are the coupling coefficients associated to M_{12}, M_{1O} and M_{2O} respectively. If we further analyse these last expressions, we can derive the changes in the resistances and the self-inductances for the equivalent circuit. In particular:

$$Real\left(Z'_{11}\right) = R'_1 = R_1 + \frac{\omega^2 M_{1O}^2}{|Z_{MO}|^2} * R_{MO} = R_1 * \beta_{R1} \quad (6)$$

$$L'_1 = L_1 - \frac{\omega^2 M_{1O}^2}{|Z_{MO}|^2} * L_{MO} = L_1 * \beta_{L1} \quad (7)$$

$$Real(Z'_{22}) = R'_2 = R_2 + \frac{\omega^2 M_{2O}^2}{|Z_{MO}|^2} * R_{MO} = R_2 * \beta_{R2} \quad (8)$$

$$L'_2 = L_2 - \frac{\omega^2 M_{2O}^2}{|Z_{MO}|^2} * L_{MO} = L_2 * \beta_{L2} \quad (9)$$

Thus, the self-inductances and the new mutual inductance of the equivalent coupler are lower than those in the configuration of the original coils without the metal object [42]. Consequently, β_M, β_{L1} and β_{L2} are lower than 1. As for the resistances, they increase, i.e. β_{R1} and β_{R2} are greater than 1. These changes alter the electrical parameters of the system and primary and secondary currents are modified along with the voltages on the coils. This is the basis of self-sensing MOD techniques.

The variations of these parameters depend on the electrical features of the metal object (L_{MO} and R_{MO}) and the relative position of the metal object in the power transfer volume (modelled by M_{1O} and M_{2O}). To see the effects, we have analysed how the inclusion of metal objects affects the wireless charger described in [43], which is SAE J2954-compliant. Fig. 3 illustrates how the inductance and the resistance affect the primary and secondary currents and voltages. For simplicity, we assume that $\beta_R = \beta_{R1} = \beta_{R2}$, $\beta_L = \beta_{L1} = \beta_{L2}$ and $\beta_M = 0.8$. It can be observed that the current and voltage on the primary side have an immediate and appreciable variation when there is an object. This phenomenon does not hold for the current on the secondary side, where these parameters are lower. From this experiment, it can be concluded that the analysis on the primary side is more effective than the study of the measurements on the secondary side.

III. ELECTRICAL MODEL OF A BEVERAGE CAN

As shown in Fig. 1, we can model the can as a conventional metal object with resistance (R_O) and self-inductance (L_O). The electrical characterization of the object consists of defining these two parameters. For this purpose, we have modelled the physical properties of the object in a FEM tool. From the model, we determine the electrical properties, which are validated with experimental tests next.

To account for the object complex geometry, a model in Ansys Maxwell was created to assess accurate values of R_O and L_O. A detailed model of the can is in Fig. 4. The use of this exact model incurs high computational times, especially when testing the can with the complete EV wireless charger. The execution of a simulation in Ansys Maxwell with the exact model of the can takes 12:00 minutes with an Intel Core i7-10700K CPU machine with a 32- Gb Kingston HyperX RAM and Samsung 980 Pro SSD PCIe X4 NVMe M.2. Working with this computational time is a relevant burden for large simulation sets, as the one required by optimization/Montecarlo analysis or machine-learning dataset creation. Thus, we have opted for a simplified version of this model, which is depicted in Fig. 5. With this simplified model, a simulation takes 6:42 minutes. Thus, the model can be used as a lightweight modelling instrument.

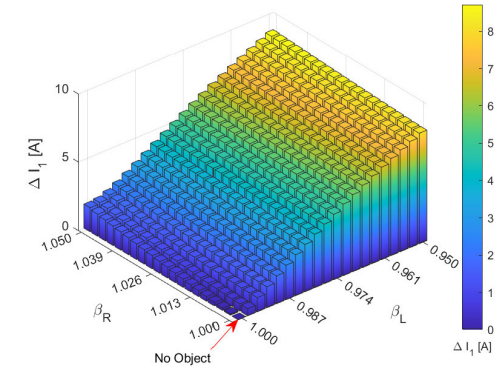

(a) Increments of I_1.

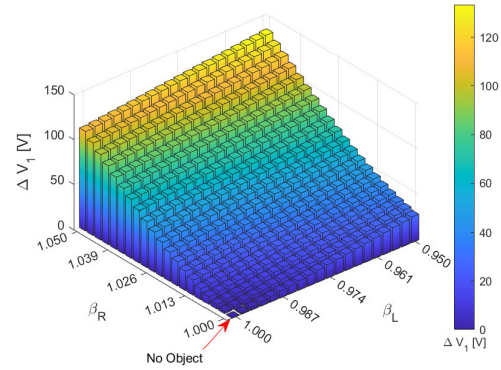

(b) Increments of V_1.

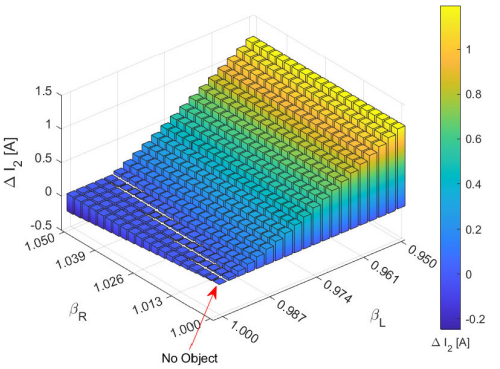

(c) Increments of I_2.

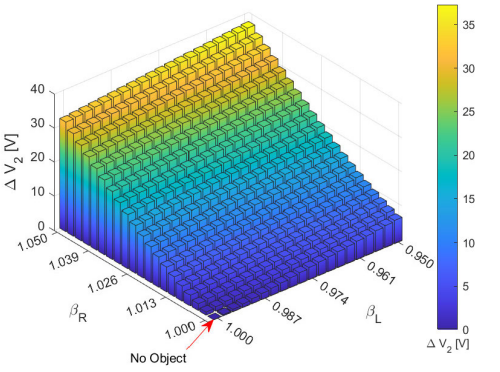

(d) Increments of V_2.

FIGURE 3. Theoretical electrical parameters depending on R and L variation due to a metal object.

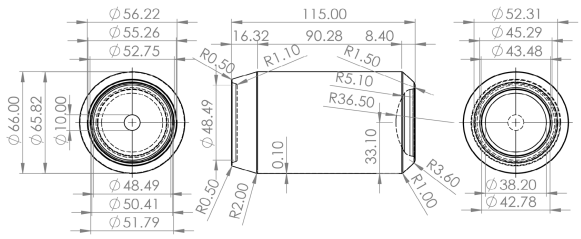

FIGURE 4. Dimensions and parts of the can.

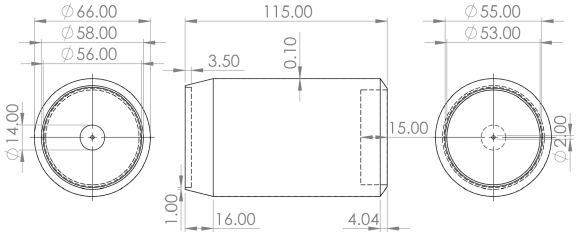

FIGURE 5. Dimensions and parts of the modelled can.

With this model, we aim to derive the electrical characterization of the beverage can provided by Ansys Maxwell. The steps which have been followed are:

i Parameterization of the model in Ansys Maxwell in order to easily change any surface if necessary. We have avoided any curved surface presented on the real can in order to minimize the simulation time.

ii Assigning a winding to the cross-section of the solid. This will act as the electrical model of the can. Please, take into account that the conventional model of a metal object is an inductance with a resistance, as depicted in Fig.1.

iii Exciting the previously mentioned winding with a 1-V alternating source, which would emulate the pulse emitted by the LCR Programmable bridge HM8118.

With this procedure, we can determine that the electrical parameters of the can are $R_O = 0.473\,m\Omega$ and $L_O = 2.6\,nH$. Moreover, the estimation of the parameters was validated through an experimental setup, measuring the actual parameters through an LCR meter. One of the difficulties encountered when measuring the resistance and inductance of the can is that this object is not composed of a single alloy. Beverage cans are composed of two different alloys. The bodies are made of aluminum alloy 3003 and the lids are composed of aluminum alloy 5182, as explained in [44]. As described in [45] and [46], the body is 97% aluminium whereas the lid is only 93.85%. The differences in the composition of these two parts of the can are expected to result in differences in their electrical characterization.

As illustrated in Fig. 6, the resistance and inductance measurements are strongly influenced by the positioning of the contacting probes. Fig. 6.a shows the results when the

parameters are measured in the body and Fig. 6.b when it is done using the lid and the bottom as connectors. It can be observed that there is a notable difference in the resistance and the inductance. Considering the resistances of the body and the lid, we have elaborated the equivalent resistive circuits in Fig. 6.c and Fig.6.d. When measuring in the body, the resistance of the lid (R_{lid}) is in parallel with that of the body (R_{body}). R_{lid} is much greater than R_{body} due to the greater resistivity of the alloy 5182 ($\rho_{5182} = 56.0\,n\Omega$) opposite to the one of the 3003 ($\rho_{3003} = 37.6\,n\Omega$) as can be seen in [47] and [48] respectively. Therefore R_{body} is dominant in this particular measurement. In contrast, when the measurement is accomplished as shown in Fig. 6.b, there is a series of electrical paths with the resistances of the lid, the body and the bottom. Considering the different orders of magnitudes of these resistances, the equivalent resistance is associated with the R_{lid}. A similar phenomenon occurs with the inductance.

In our case, we assume that it is more probable for a can to be unintentionally placed between the two coils horizontally rather than in a vertical position. Considering the magnetic flux lines of an EV wireless charger, the incidence of the electromagnetic flux is greater on the surface of the body. From Fig. 4, we can derive that the surfaces are $S_{Body} = 272.61\,cm^2$ and $S_{Lid} = 15.21\,cm^2$. Thus, the measurement where the effects of the body are more relevant is considered as a reference to check the accuracy of the model, i.e. the one from Fig. 6.b. There is a very good agreement for the inductance values. As for the resistance, the values in the laboratory are greater because the connector points used for the measurements also include a resistive part.

In this preliminary analysis, we have checked that there is a good agreement between the electrical characterization provided by Ansys Maxwell and the lab measurements. Thus, we can suggest that the model developed by Ansys Maxwell is valid. However, a more extensive study will be done based on the electrical parameters of the system with this model and with a real prototype for an EV wireless charger to confirm the validity of the electrical model. This validation is carried out in Section V with the model described in Section IV.

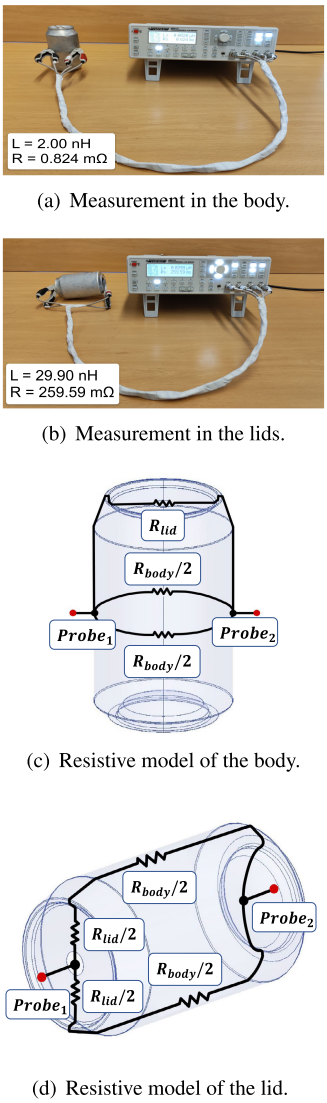

(a) Measurement in the body.

(b) Measurement in the lids.

(c) Resistive model of the body.

(d) Resistive model of the lid.

FIGURE 6. Measurement of *L* and *R* parameters of the can and equivalent resistive circuit.

IV. ELECTRICAL MODEL OF THE EV WIRELESS CHARGER

In the previous Section, a complete electrical characterization of the beverage can was assessed. The equivalent circuit derived from this characterization can now be included in further analysis on the complete electrical circuit for an EV wireless charger. This system is also composed of some additional elements, as shown in Fig. 1, which must be modelled to derive precise electrical parameters (voltages/currents on the primary and secondary sides). This modelling depends on the implementation. Considering the prototype we have in the laboratory, we have modelled:

- Primary inverter in a full-bridge topology. It is composed of two evaluation kits CREE KIT8020CRD8FF1217P-1, whose main components are MOSFET CREE C2M0080120D. We have taken into account that the on-resistance and threshold voltage are temperature-dependent. We have also modelled the parallel capacitance as a function of the drain-source voltage. These phenomena are explained in [49].
- Non-controlled rectifier with a full-bridge configuration. The four diodes are CREE C4D20120D0. We have considered that the parallel capacitance of the diodes is dependent on the reverse voltage. We have also included the dependency of the forward voltage on the forward current, as described in [50].
- A smoothing capacitor acting as a filter of the rectifier. This needs to be taken into account because it distorts the wave of the voltage of the secondary coil. It has been measured with the LCR meter and included in the electrical model.
- Wires used to connect the components, whose inductances and parallel capacitances have been measured

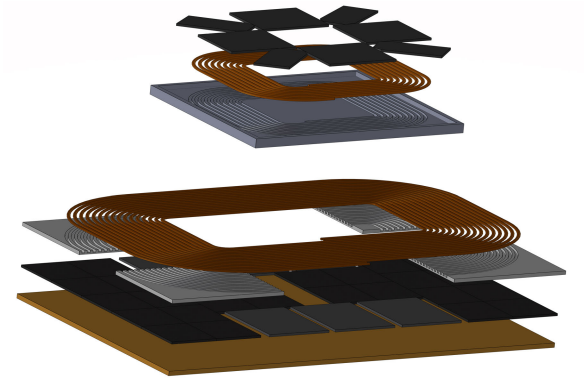

FIGURE 7. Ferromagnetic material and shielding disposition in the coils.

TABLE 3. Characteristics of the coupled coils.

Design frequency (f_o)	85 kHz
Primary coil dimensions	0.51 m × 0.66 m
Resistance of the primary coil (R_1)	97.46 mΩ
Self-inductance of the primary coil (L_1)	61.06 μH
Secondary coil dimensions	0.35 m × 0.35 m
Resistance of the secondary coil (R_2)	55.94 mΩ
Self-inductance of the secondary coil (L_2)	42.02 μH
Distance between coils assumed in the design (gd)	0.10 m

with the LCR meter. We consider that it was important to include them in the model as they can alter the phases of the electrical parameters of the system.

As for the coils, they are also modelled in Ansys Maxwell to be similar to the pair we have in the laboratory. The exact model is in Fig. 7. The features of the coils are in Table 3, which is compliant with SAE J2954. The coils are made of AWG-38 Litz wire. Both coils have a ferrite layer which improves the coupling coefficient between them, composed of tiles of dimensions $55 \times 55 \times 5\ mm^3$. On the primary side, it is constituted by a single layer under the wire. on the secondary side, they are placed following the path of the wire with a space between the tiles to achieve the maximum coupling coefficient with the less material possible. In addition, the secondary side has an aluminum foil as a shield.

A series-series compensation topology is used with $C_1 = 56.50\,nF$ and $C_2 = 82.83\,nF$. The power transferred is 500 W. As stated on SAE J2954, all measurements and modelling have been done in a thermal steady state reaching 45 °C on the transmitter components and 35 °C on the receiver elements. These conditions have been taken into account in the equivalent circuit of the power converters. The steps followed for modelling the complete EV system accurately are:

i Measurement of the impedance of the coils, compensation capacitors and wires, including the parasitic capacitance induced between the wires, which all are temperature-dependent. These prototype values are included in the model developed in Ansys Maxwell.

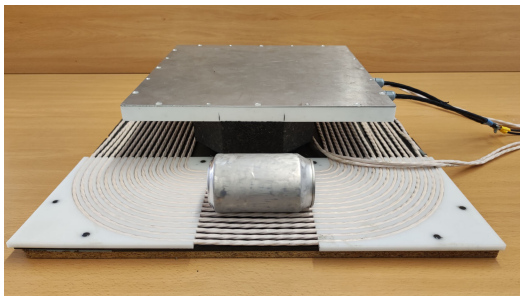

FIGURE 8. Coils with the can in the prototype.

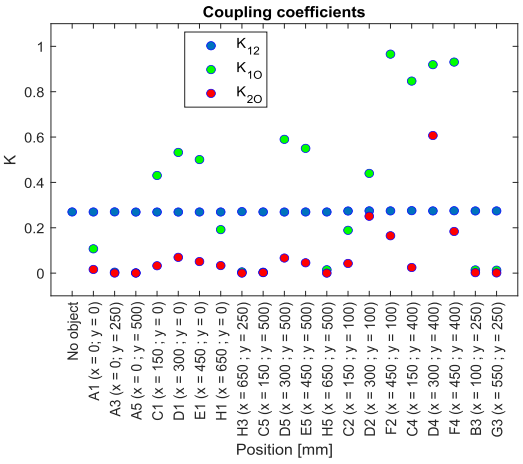

FIGURE 9. Coupling coefficients of the system for different positions of the can.

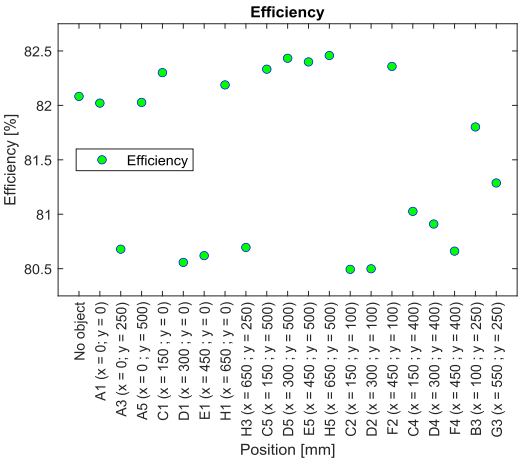

FIGURE 10. Efficiency of the system depending on the position of the can.

ii Measurement of the temperature of the components of the inverter and rectifier as their impedances are strongly influenced by it. The parameters of these parameters are modified accordingly in the software model.

V. EXPERIMENTAL VALIDATION OF THE MODEL

Once the electrical model of the beverage can has been derived, we evaluated the accuracy of using this model in a

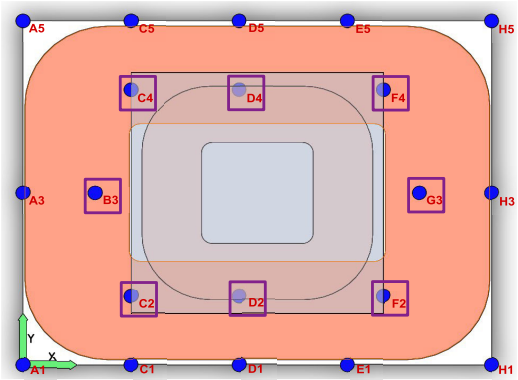

FIGURE 11. Evaluated positions of the beverage can.

MOD technique based on the study of the electrical parameters, specifically, on a self-sensing approach. Therefore, we have conducted some experimental tests on the prototype for EV wireless chargers in Fig. 8. In these tests, we varied the positions of the can and measured the current and voltage of the primary and secondary sides. We have also included the variation on the position of the can in the system, effect which has been modelled in Ansys Maxwell. For each position, the software tool indicates the mutual inductances (M_{1O}, M_{2O} and M_{12}) and the corresponding coupling coefficients (K_{1O}, K_{2O} and K_{12}). The coupling coefficients are illustrated in Fig. 9. The presence of the object does not impose a significant variation on the coupling coefficient between the power coils. On the contrary, coupling factors between the can and the coils are severely affected by the relative position of the object, which is expected to induce significant changes in the voltage and current of the coils. In particular, the variation of the coupling coefficient is more severe on the transmitter side (K_{1O} in Fig. 9). The efficiency of the system has a lower variation, as shown in Fig.10.

Using the parameters of the mutual inductances and the precise electrical model that we have described in Section IV, we can also obtain the simulated values for the voltage and current on the primary and secondary sides. Thus, we generate two data sets: (i) one based on experimental results and (ii) one using the proposed model of the can and solved as an equivalent electrical circuit in PSIM. The comparison of these two sets of electrical values can provide a helpful indicator of the accuracy of the can model.

The measurements and modelling have been conducted for the positions of the can indicated as blue circles in Fig. 11. The can is always in contact with the primary coil and in a horizontal position. The results comparing both approaches are in Fig. 12 and Fig. 13 for the primary and secondary sides respectively. For each measured value, we have a vertical bar indicating the 5% error interval. In this way, the precision of the model can be easily evaluated. It can be seen that there is a good agreement between the results derived from the model and the experimental measurements for the primary and secondary sides. The error of the model is lower than 5%,

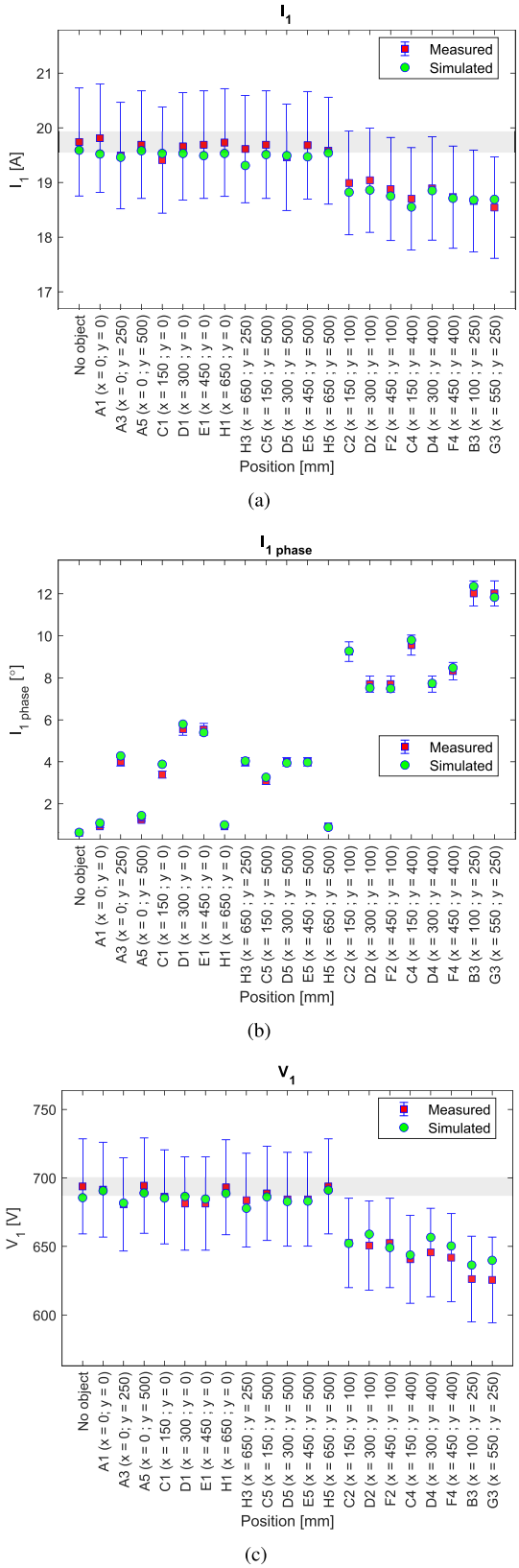

FIGURE 12. Electrical parameters of the transmitter coils deviation with 5% tolerance.

so the model derived in this paper is a useful tool to include this type of metal object in simulations.

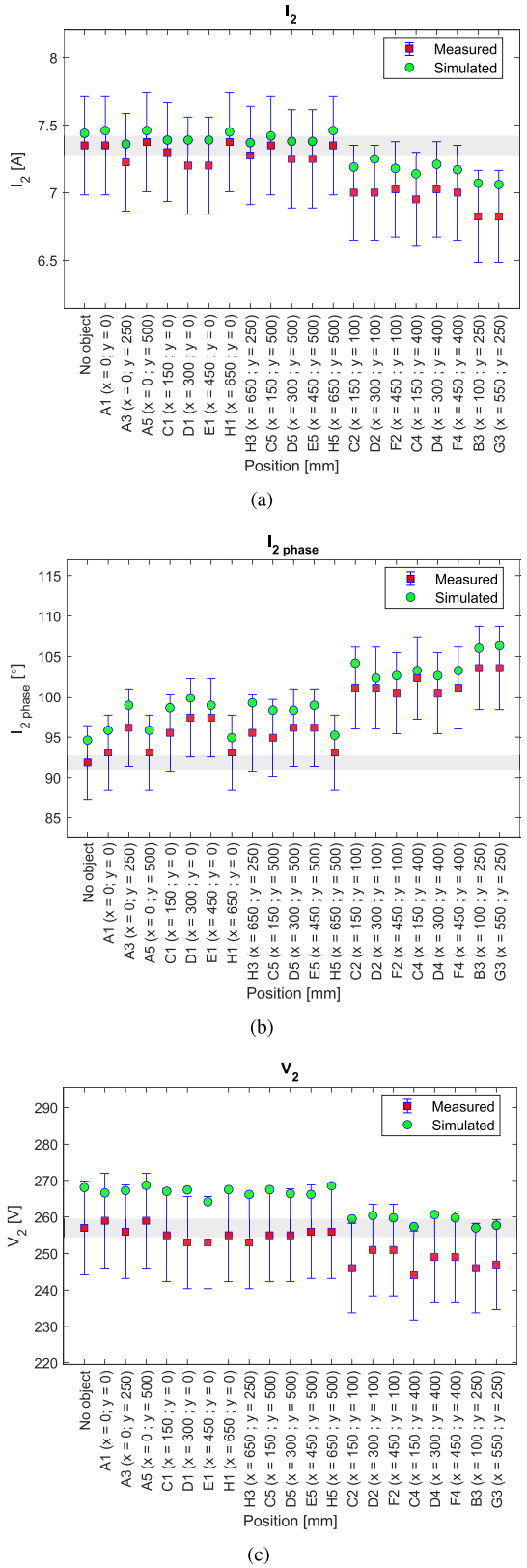

FIGURE 13. Electrical parameters of the receiver coil with 5% tolerance.

From these data, an important issue that could be evaluated is whether the analysis of the electrical parameters is useful for metal object detection, that is, a simple self-sensing approach can be applied to detect the can. We have included two horizontal lines in Fig. 12 and Fig. 13, which state the 1% error of the measurement with no object (grey area). We assume that the amplitude and phase of the voltages and currents can be measured with an error of 1%, as it is the highest precision provided by the intrumental equipment. Using the amplitude of the currents (in Fig. 12.a and Fig.13.a), we can only detect the object when it is in an area close to the secondary coil. These points are marked as black squares in Fig. 11.

A similar conclusion can be derived with the amplitude of the primary voltage. However, the phase of the currents on both the primary and secondary sides reveal themselves as good indicators of the presence of a metal object. Using a combination of different measurements with pre-processing techniques (such as feature extraction or PCA-based approaches) can further extend these thresholds. A detailed and comparative analysis of these techniques is beyond the purpose of this work. However, the modelling methodology proposed can surely be used to create data towards these kinds of investigations.

VI. CONCLUSION

This paper presents an effective model of a beverage can as a metal object in an EV wireless charger. The electrical characterization of the can is elaborated as a simple series connection of an inductance and a resistance, which are derived from the physical modelling of the can in a FEM tool. The model has been verified with lab measurements, concluding that there is a good agreement between model and experimental data. The electrical model of the can was included in a larger simulation for a WPT system to assess the macroscopic effect of the can positioning on the electrical parameters of the system, testing a wide range of positions in the power transfer area. By comparing the experimental and simulated data of this large test, we can conclude that the model for the beverage can is valid, making is useful to create large datasets required for the implementation and training of black-box FOD techniques. The analysis of the results highlights that the amplitude of the current and voltages are only useful to detect a metal object when it is close to the secondary coil. For the entire area, monitoring the phase in the primary currents is foreseen as a better self-sensing technique. Although the procedure described in this paper (physical characterization and derivation of the electrical model) is used for a can-shaped object, the same methodology could be applied to other objects, independently of their dimensions.

REFERENCES

[1] A. Trivino-Cabrera, J. M. Gonzalez-Gonzalez, and J. A. Aguado, *Wireless Power Transfer for Electric Vehicles: Foundations and Design Approach*. Cham, Switzerland: Springer, 2020.

[2] Q. Wang, W. Li, J. Kang, and Y. Wang, "Electromagnetic safety evaluation and protection methods for a wireless charging system in an electric vehicle," *IEEE Trans. Electromagn. Compat.*, vol. 61, no. 6, pp. 1913–1925, Dec. 2019.

[3] J. Lu, G. Zhu, and C. C. Mi, "Foreign object detection in wireless power transfer systems," *IEEE Trans. Ind. Appl.*, vol. 58, no. 1, pp. 1340–1354, Jan. 2022.

[4] *Wireless Power Transfer for Light-Duty Plug-In/Electric Vehicles and Alignment Methodology*, SAE International, International Standard SAE J2954 202010, 2020.

[5] S. Niu, S. Niu, C. Zhang, and L. Jian, "Blind-zone-free metal object detection for wireless EV chargers employing DD coils by passive electromagnetic sensing," *IEEE Trans. Ind. Electron.*, vol. 70, no. 1, pp. 965–974, Jan. 2023.

[6] S. Y. Chu, X. Zan, and A.-T. Avestruz, "Electromagnetic model-based foreign object detection for wireless power transfer," *IEEE Trans. Power Electron.*, vol. 37, no. 1, pp. 100–113, Jan. 2022.

[7] W. Ye, S. Wang, and N. Parspour, "A foreign object detection method using high frequency excitation for wireless power transfer," in *Proc. Wireless Power Week (WPW)*, Jul. 2022, pp. 327–331.

[8] S. Y. Jeong, V. X. Thai, J. H. Park, and C. T. Rim, "Metal object detection system with parallel-mistuned resonant circuits and nullifying induced voltage for wireless EV chargers," in *Proc. Int. Power Electron. Conf. (IPEC-Niigata -ECCE Asia)*, May 2018, pp. 2564–2568.

[9] J. Byun, S. Ann, W.-J. Son, J. H. Lee, and B. K. Lee, "Design of double-layered detection coil for metal object detection in wireless power transfer systems for electric vehicles," in *Proc. IEEE Appl. Power Electron. Conf. Exposit. (APEC)*, Mar. 2020, pp. 1617–1621.

[10] B. Long, Q. Zhu, and A. P. Hu, "Analysis of transimpedance variation and its potential application for metal object detection in inductive power transfer systems," in *Proc. Wireless Power Week (WPW)*, Jul. 2022, pp. 585–588.

[11] C. Liu, H. Chen, Z. Cheng, Y. Lin, J. Wu, and X. He, "Convolutional neural network based metal object detection system for wireless EV charging," in *Proc. IEEE Energy Convers. Congr. Exposit. (ECCE)*, Oct. 2022, pp. 1–5.

[12] Y. Zhang, B. Yu, K. Wang, Y. Wang, and Y. Yang, "Metal foreign object detection in electric vehicle wireless power transmission," in *Proc. IEEE Int. Conf. Inf. Technol., Big Data Artif. Intell. (ICIBA)*, vol. 1, Nov. 2020, pp. 696–701.

[13] T. Zhou, Y. Sun, Y. Lan, and K. Song, "Metal foreign object detection algorithm based on multivariate normal distribution for wireless power transfer system," in *Proc. Wireless Power Week (WPW)*, Jul. 2022, pp. 722–727.

[14] Y. Sun, G. Wei, K. Qian, P. He, C. Zhu, and K. Song, "A foreign object detection method based on variation of quality factor of detection coil at multi-frequency," in *Proc. IEEE 12th Energy Convers. Congr. Exposit. Asia (ECCE-Asia)*, May 2021, pp. 1578–1582.

[15] Y. Gong, Y. Otomo, and H. Igarashi, "Neural network for both metal object detection and coil misalignment prediction in wireless power transfer," *IEEE Trans. Magn.*, vol. 58, no. 9, pp. 1–4, Sep. 2022.

[16] J. Pávó, Z. Badics, S. Bilicz, and S. Gyimóthy, "Efficient perturbation method for computing two-port parameter changes due to foreign objects for WPT systems," *IEEE Trans. Magn.*, vol. 54, no. 3, pp. 1–4, Mar. 2018.

[17] A. Ramezani, S. Wang, and M. Perry, "A misalignment tolerant foreign object detection for EV wireless charging applications," in *Proc. IEEE Wireless Power Technol. Conf. Expo (WPTCE)*, Jun. 2023, pp. 1–5.

[18] J. Xiao, X. Guo, H. Shi, P. Bai, W. Gong, and C. Tang, "Method of non-blind-zone foreign object detection in wireless power transfer system," in *Proc. IEEE 9th Int. Conf. Power Electron. Syst. Appl. (PESA)*, Sep. 2022, pp. 1–6.

[19] M. Li, W. Zhong, and J. Meng, "Research on foreign object detection in WPT system based on power spectrum estimation of transmitter current," in *Proc. 34th Chin. Control Decis. Conf. (CCDC)*, Aug. 2022, pp. 683–687.

[20] D. G. Lee, D. Y. Um, S. A. Chae, and G. S. Park, "Foreign object detection in wireless power transfer using sensing coils," in *Proc. IEEE 5th student Conf. Electric Mach. Syst. (SCEMS)*, Nov. 2022, pp. 1–4.

[21] L. Xiang, Z. Zhu, J. Tian, and Y. Tian, "Foreign object detection in a wireless power transfer system using symmetrical coil sets," *IEEE Access*, vol. 7, pp. 44622–44631, 2019.

[22] Y. Sun, K. Song, T. Zhou, G. Wei, Z. Cheng, and C. Zhu, "A shared method of metal object detection and living object detection based on the quality factor of detection coils for electric vehicle wireless charging," *IEEE Trans. Instrum. Meas.*, vol. 72, pp. 1–17, 2023.

[23] T. Sun and C. Qi, "Design of metal object detection coil set with positioning function for WPT system," in *Proc. IECON 46th Annu. Conf. IEEE Ind. Electron. Soc.*, Oct. 2020, pp. 3884–3888.

[24] V. X. Thai, J. H. Park, S. Y. Jeong, C. T. Rim, and Y.-S. Kim, "Equivalent-circuit-based design of symmetric sensing coil for self-inductance-based metal object detection," *IEEE Access*, vol. 8, pp. 94190–94203, 2020.

[25] J. Wang, J. Gao, A. Yang, and J. Zhou, "Impedance identification-based foreign object detection for wireless power transfer system," in *Proc. IEEE 31st Int. Symp. Ind. Electron. (ISIE)*, Jun. 2022, pp. 895–898.

[26] H. Jafari, M. Moghaddami, and A. I. Sarwat, "Foreign object detection in inductive charging systems based on primary side measurements," *IEEE Trans. Ind. Appl.*, vol. 55, no. 6, pp. 6466–6475, Nov. 2019.

[27] S. Li, H. Li, Z. Wu, G. Bao, K. Qian, and Y. Li, "Foreign object detection for LCC-S wireless power transfer system based on LSTM," in *Proc. IEEE Int. Conf. Emergency Sci. Inf. Technol. (ICESIT)*, Nov. 2021, pp. 165–169.

[28] M. Moghaddami and A. I. Sarwat, "A sensorless conductive foreign object detection for inductive electric vehicle charging systems based on resonance frequency deviation," in *Proc. IEEE Ind. Appl. Soc. Annu. Meeting (IAS)*, Sep. 2018, pp. 1–6.

[29] S. Son, S. Lee, J. Rhee, Y. Shin, S. Woo, S. Huh, C. Lee, and S. Ahn, "Foreign object detection of wireless power transfer system using sensor coil," in *Proc. IEEE Wireless Power Transf. Conf. (WPTC)*, Jun. 2021, pp. 1–4.

[30] M. Kuzmin, E. Zanganeh, G. Baranov, A. Tsyrinova, P. Smirnov, A. Zolotarev, and P. Kapitanova, "Experimental investigation of metasurface-based resonator for one-to-many wireless power transfer systems in the presence of foreign objects," *Photon. Nanostruct. Fundamentals Appl.*, vol. 56, Sep. 2023, Art. no. 101155.

[31] S. Niu, C. Zhang, Y. Shi, S. Niu, and L. Jian, "Foreign object detection considering misalignment effect for wireless EV charging system," *ISA Trans.*, vol. 130, pp. 655–666, Nov. 2022.

[32] Y. Li, Q. Zhang, X. Liu, N. Xiao, P. Ning, and Y. Li, "Metal foreign body detection based on double/multiple differential coils pair magnetic module," *J. Magn. Magn. Mater.*, vol. 559, Oct. 2022, Art. no. 169542.

[33] S. Zhao, C. Xia, Z. Yang, H. Lu, H. Zhang, and C. Lu, "Bipolar checkerboard metal object detection without blind zone caused by excitation magnetic field for stationary EV wireless charging system," *IEEE Trans. Power Electron.*, vol. 38, no. 5, pp. 6696–6709, May 2023.

[34] S. Niu, Q. Zhao, H. Chen, S. Niu, and L. Jian, "Noncooperative metal object detection using pole-to-pole EM distribution characteristics for wireless EV charger employing DD coils," *IEEE Trans. Ind. Electron.*, early access, Jul. 18, 2023, doi: 10.1109/TIE.2023.3292870.

[35] V. X. Thai, G. C. Jang, S. Y. Jeong, J. H. Park, Y.-S. Kim, and C. T. Rim, "Symmetric sensing coil design for the blind-zone free metal object detection of a stationary wireless electric vehicles charger," *IEEE Trans. Power Electron.*, vol. 35, no. 4, pp. 3466–3477, Apr. 2020.

[36] W. Cai, F. Yi, and L. Jiang, "Fast online foreign object detection method using auxiliary coils in wireless charging systems," in *Proc. IEEE Transp. Electrific. Conf. Expo (ITEC)*, Jun. 2020, pp. 979–984.

[37] Y. Deguchi, S. Nagai, T. Fujita, H. Fujimoto, and Y. Hori, "Sensorless metal object detection using transmission-side voltage pulses in standby phase for dynamic wireless power transfer," in *Proc. IEEE PELS Workshop Emerg. Technol., Wireless Power Transf. (WoW)*. Union City, NJ, USA: Wire, Jun. 2021, pp. 1–5.

[38] N. Kuyvenhoven, C. Dean, J. Melton, J. Schwannecke, and A. E. Umenei, "Development of a foreign object detection and analysis method for wireless power systems," in *Proc. IEEE Symp. Product Compliance Eng.*, Oct. 2011, pp. 1–6.

[39] T. Imura, "Simple equivalent circuit model with foreign object on wireless power transfer via magnetic resonant coupling," in *Proc. IEEE Conf. Antenna Meas. Appl. (CAMA)*, Dec. 2017, pp. 367–370.

[40] V.-B. Vu, A. Ramezani, A. Triviño, J. M. González-González, N. B. Kadandani, M. Dahidah, V. Pickert, M. Narimani, and J. Aguado, "Operation of inductive charging systems under misalignment conditions: A review for electric vehicles," *IEEE Trans. Transport. Electrific.*, vol. 9, no. 1, pp. 1857–1887, Mar. 2023.

[41] A. Triviño-Cabrera, J. M. González-González, and J. A. Aguado, "Design and implementation of a cost-effective wireless charger for an electric bicycle," *IEEE Access*, vol. 9, pp. 85277–85288, 2021.

[42] J. Kim, J. Kim, S. Kong, H. Kim, I.-S. Suh, N. P. Suh, D.-H. Cho, J. Kim, and S. Ahn, "Coil design and shielding methods for a magnetic resonant wireless power transfer system," *Proc. IEEE*, vol. 101, no. 6, pp. 1332–1342, Jun. 2013.

[43] J. M. González-González, A. Triviño-Cabrera, and J. A. Aguado, "Model predictive control to maximize the efficiency in EV wireless chargers," *IEEE Trans. Ind. Electron.*, vol. 69, no. 2, pp. 1244–1253, Feb. 2022.

[44] G.T. Kridli, P.A. Friedman, and J.M. Boileau, "Chapter 7—Manufacturing processes for light alloys," *Materials, Design and Manufacturing for Lightweight Vehicles* (Woodhead Publishing in Materials), 2nd ed., J. M. Boileau and P. K. mallick, Eds. Sawston, Cambridge: Woodhead Publishing, 2021, pp. 267–320.
[45] C. Vargel, "Chapter G.3—3xxx series alloys," in *Corrosion Aluminium (Second Edition)*, 2nd ed., C. Vargel, Ed. Amsterdam, The Netherlands: Elsevier, 2020, pp. 465–468.
[46] C. Vargel, "Chapter G.4—5xxx series alloys," in *Corrosion Aluminium (Second Edition)*, 2nd ed., C. Vargel, Ed. Amsterdam, The Netherlands: Elsevier, 2020, pp. 469–484.
[47] L. Gong, Y. Xi, Z.-R. Ma, and C.-L. Liu, "Modeling, identification and simulation of DC resistance spot welding process for aluminum alloy 5182," *J. Shanghai Jiaotong Univ. Sci.*, vol. 18, no. 1, pp. 101–104, Feb. 2013.
[48] W. X. Wang, J. X. Zhang, Z. J. Wang, and W. C. Liu, "A comparative study of the transformation kinetics of recrystallization texture of CC and DC 3003 aluminum alloys," *Mater. Characterization*, vol. 141, pp. 412–422, Jul. 2018.
[49] *C2m0080120d Silicon Carbide Power MOSFET C2M TM MOSFET*.
[50] *C4d20120d Silicon Carbide Schottky Diode Z-Rec*.

ALICIA TRIVIÑO received the master's degree in telecommunication engineering and in computer science engineering from the University of Málaga, Spain, in 2002 and 2008, respectively. Her thesis, which was defended, in 2007, focused on wireless networks.

She currently holds a position as an Associate Professor with the University of Málaga. Her research interest includes wireless power transfer. In the area related to electric vehicles wireless chargers, she has actively participated in the design and development of several prototypes, including features as bi-directionality and dynamic charge.

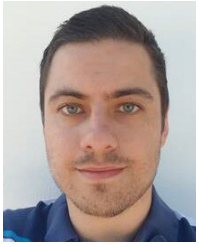

ELISEO VILLAGRASA was born in Málaga, Spain. He received the B.Sc. degree in industrial technologies from the University of Málaga, Spain, in 2020, where he is currently pursuing the double master's degree in industrial and mechatronics engineering.

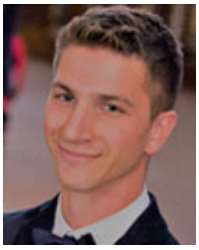

FABIO CORTI (Member, IEEE) received the M.S. degree in electrical and automation engineering and the Ph.D. degree in industrial engineering from the University of Florence, Italy, in 2016 and 2019, respectively. He was a Postdoctoral Research Fellow with Consiglio Nazionale delle Ricerche (CNR), in 2020. He is currently a Postdoctoral Research Fellow with the University of Perugia. His research interests include modeling and control of DC–DC PWM and resonant converters, wireless power transfer, and electric vehicle powertrain.

GABRIELE MARIA LOZITO (Member, IEEE) received the master's degree in electronics engineering and the Ph.D. degree in soft computing techniques on embedded systems from the University of Roma Tre, in 2010 and 2016, respectively. He was a Visiting Researcher with the National Physical Laboratory (NPL), London. He is currently an Assistant Professor with the University of Florence on the main research topic of circuit modeling for renewable energy applications. He has published his research in several international journals. His research interests include machine learning and optimization algorithms, embedded devices implementations, and magnetic materials modeling.

ALBERTO REATTI (Member, IEEE) received the M.Sc. degree in electronics engineering from the University of Florence, Italy, in 1988, and the Ph.D. degree in electrical engineering from the University of Bologna, Italy, in 1993. In 1992, he was an Associate Researcher with the Department of Electrical Engineering, Wright State University, Dayton, OH, USA. He has been an Associate Professor with the Department of Information Engineering, since 2000, and the President of Patent and Technology Transfer Board of the University of Florence. He has coauthored more than 100 papers, including those appeared in IEEE TRANSACTIONS and journals. He holds two patents. His current research interests include high-frequency resonant and PWM DC–DC power converters, modeling, and control of converters and renewable power sources.

Open Access funding provided by 'Università degli Studi di Firenze' within the CRUI CARE Agreement